Hydrol. Earth Syst. Sci. Discuss., 11, 12833–12882, 2014
www.hydrol-earth-syst-sci-discuss.net/11/12833/2014/
doi:10.5194/hessd-11-12833-2014

Hydrology and Earth System Sciences
Discussions
Open Access

Topographic controls on soil moisture scaling properties in polygonal ground using idealized high-resolution surface–subsurface simulations

G. Bisht and W. J. Riley

Earth Science Division, Lawrence Berkeley National Laboratory, 1 Cyclotron Road, Berkeley, California 94720, USA

Received: 10 October 2014 – Accepted: 25 October 2014 – Published: 18 November 2014

Correspondence to: G. Bisht (gbisht@lbl.gov)

Published by Copernicus Publications on behalf of the European Geosciences Union.

Abstract

Microtopographic features, such as polygonal ground, are characteristic sources of landscape heterogeneity in the Alaskan Arctic coastal plain. Here, we analyze the hypothesis that microtopography is a dominant controller of soil moisture in polygonal landscapes. We perform multi-year surface–subsurface isothermal flow simulations using the PFLOTRAN model for summer months at six spatial resolutions (0.25–8 m, in increments of a factor of 2). Simulations are performed for four study sites near Barrow, Alaska that are part of the NGEE-Arctic project. Results indicate a non-linear scaling relationship for statistical moments of soil moisture. Mean soil moisture for all study sites is accurately captured in coarser resolution simulations, but soil moisture variance is significantly under-estimated in coarser resolution simulations. The decrease in soil moisture variance in coarser resolution simulations is greater than the decrease in soil moisture variance obtained by coarsening out the fine resolution simulations. We also develop relationships to estimate the fine-resolution soil moisture probability distribution function (PDF) using coarse resolution simulations and topography. Although the estimated soil moisture PDF is underestimated during very wet conditions, the moments computed from the inferred soil moisture PDF had good agreement with the full model solutions (bias $< \pm 4\,\%$ and correlation > 0.99) for all four sites. Lastly, we develop two spatially-explicit methods to downscale coarse-resolution simulations of soil moisture. The first downscaling method requires simulation of soil moisture at fine and coarse resolution, while the second downscaling approach uses only topographical information at the two resolutions. Both downscaling approaches are able to accurately estimate fine-resolution soil moisture spatial patterns when compared to fine-resolution simulations (mean error for all study sites are $< \pm 1\,\%$), but the first downscaling method more accurately estimates soil moisture variance.

HESSD
11, 12833–12882, 2014

G. Bisht and W. J. Riley

Title Page
Abstract | Introduction
Conclusions | References
Tables | Figures
◂ | ▸
Back | Close
Full Screen / Esc
Printer-friendly Version
Interactive Discussion

1 Introduction

Northern permafrost soil currently contains approximately 1700 billion metric tons of frozen organic carbon (Tarnocai et al., 2009). Global climate is warming (Stocker et al., 2013), and "Arctic amplification" is predicted to cause disproportionately larger temperature increases at high latitudes (Holland and Bitz, 2003). This warming will cause permafrost thaw and decomposition, leading to CO_2 and CH_4 emissions to the atmosphere. There is, however, a range of estimates regarding how rapidly permafrost thaw and decomposition will occur (Koven et al., 2011; Schaefer et al., 2011; Schuur and Abbott, 2011).

Soil moisture, θ, is one of the key environmental factors controlling the rate and products (i.e., CO_2 vs. CH_4) of microbial decomposition of thawed soil organic carbon (Schuur et al., 2008). Properties of the underlying permafrost in the Arctic have been shown to control changes in soil moisture. Observational studies have documented both increases and decreases of soil moisture in Alaska due to climate change. Based on analysis of remotely sensed data from 1950–2002, Riordan et al. (2006) found significant reduction in the number and area of shallow, closed-basin ponds in regions of discontinuous permafrost, but negligible change for ponds in continuous permafrost. Jorgenson et al. (2006) analyzed areal photographs from 1945, 1982, and 2001, and found large increases in degradation of ice-wedges in continuous permafrost of northern Alaska. Since CH_4 emissions are very sensitive to soil moisture status (Torn and Chapin Iii, 1993) and have 25 times higher greenhouse warming potential on a century timescale than CO_2 (Bridgham et al., 1998), developing approaches to characterize soil moisture dynamics across a wide range of spatial scales is critical for predicting interactions between high-latitude terrestrial ecosystems and climate.

Large portions of the Arctic are characterized by polygonal ground features, which are formed due to thermal expansion and contraction of ice wedges within the soil (Hinkel et al., 2005). Polygons are classified as "low-centered" or "high-centered" based on the relationship between their central and mean elevations. Polygonal ground fea-

HESSD
11, 12833–12882, 2014

tures are dynamic components of the Arctic landscape in which ice-wedge thaw under low-centered polygon rims leads to subsidence and eventually ($\sim$ o(centuries)) to high-centered polygons (Seppala et al., 1991). Microtopography of polygonal ground influences soil hydrologic and thermal conditions (Engstrom et al., 2005). In addition to controlling CO_2 and CH_4 emissions, soil moisture impacts (1) partitioning of incoming radiation into latent, sensible, and ground heat fluxes (Hinzman and Kane, 1992; McFadden et al., 1998), (2) photosynthesis rates (Oberbauer et al., 1991; Oechel et al., 1993; McGuire et al., 2000; Zona et al., 2011), and (3) vegetation distributions (Wiggins, 1951). Non-vascular plants (mosses and lichens), which are abundant in Arctic ecosystems, contribute up to 75 % of evaporative losses (Miller et al., 1976) and are strongly influenced by near surface hydrologic conditions (Williams and Flanagan, 1996).

The recognition that soil moisture dynamics occur across a wide range of spatial scales (i.e., soil pore, Childs, 1940 to continental, Brocca et al., 2010; Li and Rodell, 2013) has motivated a large literature attempting to integrate relationships of soil moisture heterogeneity with topographic, biological, and forcing controls. Numerous studies have identified statistical self-similarity of soil moisture across a range of spatiotemporal scales via field observations and numerical experiments. A soil moisture field is self-similar if (Dubayah et al., 1997):

$$\mathbb{E}\left[\theta^q\left(A_i\right)\right] = \left(\frac{A_j}{A_i}\right)^{K(q)} \mathbb{E}\left[\theta^q(A_j)\right] \tag{1}$$

where q is the order of the moment, $K(q)$ is a set of scaling exponents associated with the moment, A_i and A_j represent fine and coarse scale areas or resolutions, respectively, and the ratio A_j/A_i is called the scale parameter λ. If $K(q)$ is a linear function, then the qth moment of soil moisture is said to exhibit simple or linear scaling, otherwise soil moisture exhibits multi-scaling. By analyzing passive microwave remotely sensed soil moisture data from 30 m to 4.4 km, Rodriguez-Iturbe et al. (1995) and Hu et al. (1997) found that soil moisture variance, σ_θ^2, exhibited a simple scaling processes. In contrast, Nykanen and Foufoula-Georgiou (2001) demonstrated a non-linear scaling

HESSD
11, 12833–12882, 2014

relationship for variability in soil moisture using data from the 1997 Southern Great Plains Hydrology Experiments (SGP97). Many observational studies have also examined the relationship between the coefficient of variation of soil moisture, C_v, and mean soil moisture, $\overline{\theta}$, and found an inverse (Famiglietti et al., 1999, 2008; Kumar, 2004) or upward convex (Brocca et al., 2010, 2012; Choi and Jacobs, 2011) relationship. Ivanov et al. (2010) used an ecohydrologic model to demonstrate a hysteretic dependence between C_v and $\overline{\theta}$ that arises because of mean and variability in soil moisture initial conditions, and the initiation of lateral subsurface fluxes. Gebremichael et al. (2009) compared scaling characteristics of simulated and observed θ fields for SGP97 as a metric for model validation and concluded that, although the model was successful in capturing total streamflow, the mechanism for runoff production was incorrectly modeled.

Numerical studies have investigated the importance of including spatial variability on model predictions. Sivapalan and Woods (1995) showed that subgrid variability of rainfall and soil moisture can have significant impact on land surface fluxes. Choi et al. (2007) demonstrated that subgrid variability impacts mean soil moisture predictions under relatively dry conditions. Jana and Mohanty (2012a) found that power-law scaling of soil hydraulic parameters allowed accurate prediction of subgrid topographic effects for four different hillslope configurations. However, there remains limited understanding of sub-meter scale soil moisture heterogeneity arising due to polygonal ground features in Arctic ecosystems (Chapin III et al., 2002).

Given the importance of soil moisture spatial heterogeneity on hydrological and biogechemical dynamics, watershed to global-scale models have integrated several approaches to account for the relevant processes, including: (1) using a non-spatially explicit tiling approach (Oleson, 2013), (2) employing effective parameters at coarse resolution (Jana and Mohanty, 2012b), and (3) modifying the governing equations to explicitly include terms related to soil moisture variance (Choi et al., 2007; Kumar, 2004). We note that the third approach could also include terms related to higher-order moments, but we are not aware of such efforts in the literature.

HESSD
11, 12833–12882, 2014

We analyzed here another approach to represent subgrid hydrological heterogeneity in models; i.e., developing relationships (i.e., reduced order models (ROMs)) between the mean properties (which could be estimated with a coarser-resolution model) and either the statistical (Riley and Shen, 2014) or spatially explicit (Pau et al., 2014) properties of the field of interest (here θ). The ROMs could be made extensible if they could be shown to be relatively invariant functions of the system properties, e.g., topographical indices, vegetation properties, or soil properties.

This study had three primary objectives: (1) characterize spatial scaling of soil moisture heterogeneity in the presence of polygonal ground features for an Arctic ecosystem, (2) develop reduced order models that allow prediction of higher-order statistical moments of soil moisture given coarse-resolution model simulations, and (3) identify controlling properties of the relationships between spatial heterogeneity and spatial resolution of predicted soil moisture fields as a first step toward representing spatial soil moisture heterogeneity in a coarser-resolution model. To address these objectives we performed multi-year surface–subsurface isothermal flow simulations using the PFLOTRAN model for summer months at multiple spatial resolutions. Descriptions of the study site, climate forcing, and model setup are presented in Sect. 2. Results of our spatial scaling analysis are presented in Sect. 3. We conclude with discussion, limitations of our approach, and observations and model structures required to overcome those shortcomings in the future.

2 Methodology

2.1 Study area

In order to reduce uncertainty regarding impacts of climate change in high-latitude ecosystems, a long term Department of Energy (DOE) Next-Generation Ecosystem Experiment (NGEE-Arctic) project was initiated with sites located near Barrow, Alaska (71.3° N, 156.5° W). Four primary NGEE-Arctic study sites (A, B, C, D; Fig. 1are located within the Barrow Environmental Observatory (BEO), which is situated on the Alaskan Coastal Plain. Mean air temperature and precipitation for Barrow, AK during summer months (July–August) are 3.3 °C and 72 mm, respectively (Liljedahl et al., 2011). The BEO has continuous permafrost (Brown et al., 1980) with land surface characterized by thaw lakes, drained thaw lake basins, and interstitial polygons (Hinkel et al., 2007). The seasonal thaw depth (active layer depth) ranges between 30–90 cm in thickness (Hinkel et al., 2003). The overall topographic relief for the BEO is low, but the four NGEE study sites have distinct microtopraphic features that include: low-centered (A), high-centered (B), and transitional polygons (C, D) (Table 1). Contrasting polygon types are indicative of different stages of permafrost degradation and were the primary motivation behind the choice of study sites for the NGEE-Arctic project. LIDAR Digital Elevation Model (DEM) data was available at 0.25 m resolution for the region encompassing all four NGEE sites.

2.2 Model

In this study we used the PFLOTRAN model, an open-source subsurface flow and reactive transport model (Hammond et al., 2012), which we modified to include surface flow. Subsurface reactive flows and transport processes in PFLOTRAN are solved using implicit time integration and finite volume spatial discretization. PFLOTRAN uses the Portable Extensible Toolkit for Scientific Computation (PETSc) libraries (Balay et al., 2013) for parallelization and domain decomposition.

We sequentially coupled a 2-D diffusion-wave overland flow model with PFLOTRAN:

$$\frac{\partial h}{\partial t} + \frac{\partial (hu)}{\partial x} + \frac{\partial (hv)}{\partial y} = S \tag{2}$$

where h is depth of surface water [m]; u and v are velocities [m s^{-1}] in x and y directions, respectively; and S is the source term [m s^{-1}]. The water velocity in x direction is computed using Manning's formula (Manning, 1891):

$$u = -\mathrm{sgn}\left(H_{i+1,j} - H_{i,j}\right) \frac{h_{i+1/2,j}^{\frac{2}{3}}}{n_\mathrm{m}} \left| \frac{H_{i+1,j} - H_{i,j}}{x_{i+1,j} - x_{i,j}} \right|^{\frac{1}{2}} \tag{3}$$

where $H(=h+z)$ is total water head [m], z is surface elevation [m], and n_m is the Manning's coefficient. The velocity in the y direction can be computed similarly. The overland flow model uses a finite volume spatial discretization and a forward Euler time integration scheme and transports surface water laterally within the domain until the surface–subsurface coupling time is reached. Then, using continuity of pressure at the surface–subsurface interface, infiltration or exfiltration is calculated. In this study, we choose 15 min as the coupling time between surface–subsurface based on a sensitivity study that minimized computational expense while maintaining accuracy of the numerical solution.

2.3 System characterization and climate forcing

Polygonal ground regions in Arctic ecosystems are also characterized by fine-scale variation in soil texture across the polygon centers, rims, and troughs (Quinton and Marsh, 1998). Troughs and centers of low-center polygons allow for preferential infiltration during the thaw season, which in turn leads to zonation of vegetation types across polygonal features (Minke et al., 2009). Apart from horizontal variability in soils due to surface features, cryoturbation leads to vertical heterogeneity in Arctic soils. Cryoturbation is a physical process of mixing soil material due to freeze–thaw cycles of ice wedges, which causes near surface soil to move downwards and deeper soil to move upwards with a time scale of hundreds of years (Bockheim, 2007). Koven et al. (2009) have shown inclusion of cryoturbative mixing within a terrestrial carbon cycle model leads to a better agreement between model predictions and observations of bulk soil organic matter and ^{14}C. Due to a lack of data to represent horizontal heterogeneity in soils at our study sites, we assumed horizontally homogeneous soil properties. Vertical soil heterogeneity is accounted for within our simulations using data reported at three depths (0–5, 5–10, and 20–25 cm) (Hinzman et al., 1991). Since our focus is on thaw period soil moisture heterogeneity over a decade, we did not account for heterogeneity arising from cryoturbation in this study.

The following van Genuchten (1980) relationship was used to approximate observations reported in Hinzman et al. (1991) of capillary pressure and hydraulic conductivity as a function of water saturation given by,

$$\theta(\psi) = \begin{cases} \theta_r + \dfrac{\theta_s - \theta_r}{\left[1+(\alpha|\psi|)^n\right]^{1-\frac{1}{n}}}, & \psi < 0 \\ \theta_s, & \psi \geq 0 \end{cases} \tag{4}$$

$$K_r(\psi) = K_{sat} s_e^2 \left\{1 - \left[1 - s_e^{\frac{1}{m}}\right]^m\right\} \tag{5}$$

$$s_e = \frac{\theta - \theta_r}{\theta_s - \theta_r} \tag{6}$$

where θ, θ_s, and θ_r are soil moisture, saturated soil moisture (or porosity) and residual soil moisture, respectively; ψ is capillary pressure [m]; α is a parameter related to air entry pressure [m^{-1}]; K_{sat} is saturated hydraulic conductivity ($cm\,min^{-1}$), and $m(= 1 - 1/n)$ and n are empirical constants. Table 2 summarizes the values of van Genuchten parameters used in this study, while Fig. 2 shows comparison of data reported in Hinzman et al. (1991) and the fitted van Genuchten model.

Boundary conditions (BCs) for the surface domain included precipitation and snowmelt while evapotranspiration (ET) was applied as a sink term for the subsurface domain. BCs for PFLOTRAN were obtained by running an offline Community Land Model (CLM4.5) simulation using meteorological data (1998–2002) from the Ameriflux station in Barrow, AK (shown in Fig. 3). A 3000 years CLM4.5 simulation was performed to allow for subsurface biogeochemistry in the model to reach equilibrium and then hourly output was saved for PFLOTRAN simulations. The ET sink was distributed

HESSD
11, 12833–12882, 2014

vertically within the PFLOTRAN subsurface domain using the same exponential rooting profile applied in CLM4.5 for Arctic shrubs (Oleson, 2013). Because of a lack of observations, no horizontal heterogeneity in vegetation type was accounted for in this study.

2.4 Simulation setup

We performed 5 year multi-resolution PFLOTRAN surface–subsurface simulations to characterize soil moisture scaling for our four NGEE-Arctic study sites. The finest resolution PFLOTRAN meshes for all four sites were created starting with 0.25 m LIDAR DEM data and comprised of prismatic grid cells with planar surface area of 3.12×10^{-2} [m^2] (= $1/2 \times 0.25\,\mathrm{m} \times 0.25\,\mathrm{m}$). The horizontal extent of the finest scale meshes was 104 m with 346 122 cells and we used 10 equally-spaced vertical layers reaching a depth of 50 cm. Additional experiments were performed at each of the four NGEE-Arctic study sites using meshes created from coarsened DEM data at 0.5, 1, 2, 4, and 8 m and an example of coarse resolution DEM for site B and D are shown in Fig. 4. The first two near-surface soil layers were assigned van Genuchten parameters corresponding to the 0–5 and 5–10 cm data, respectively, and the remaining eight layers were assigned soil parameters corresponding to data from 20–25 cm (Hinzman et al., 1991).

3 Results and discussion

We perform several analyses of the simulation outputs: (1) characterize the relationships between soil moisture moments and spatial resolution of the simulations, (2) investigate how these relationships changed when coarser-resolution simulations are used instead of spatially averaging the finest-resolution simulation (3) develop analytical approximations to relate 2nd, 3rd, and 4th statistical moments with the mean moisture, (4) investigate the topographic controls on the soil moisture probability density function, and (5) develop a method to combine the coarse-resolution simulation predictions and the fine-resolution topographic information to dynamically estimate the fine-resolution soil moisture probability distribution function.

3.1 Time series analysis

Across the four sites and five years of simulation, the coarse-resolution PFLOTRAN simulations show that soil moisture in sites A and B are comparable and relatively drier, site C is intermediate, and site D is the wettest (Fig. 5. Time series of simulated mean soil moisture for the four NGEE-Arctic study sites.) Predicted soil moisture decreased in the first half of each year except 2000, corresponding to a net loss associated with evapotranspiration. All sites became wetter starting in mid July (2001) and mid August (1998, 1999, 2000, and 2002) corresponding to increasing precipitation inputs (Fig. 3). The relatively smaller drydown period in 2000 following initial saturation occurred because of much higher precipitation in the beginning of the summer season.

The coarse-resolution simulations are able to capture the mean of the fine-resolution soil moisture ($\overline{\theta}$) accurately, with average differences of $< 1\,\%$ across all four sites and years. For brevity, we present this first analysis of simulation results at Site A for 1999, but our conclusions are applicable to all sites and for the entire simulation period. Soil moisture variance (σ_θ^2) decreased during dry-down periods and increased immediately after rainfall events (Fig. 6 shows predictions with mesh resolutions of 0.25, 2, and 8 m). The lower variance in coarser-resolution simulations compared to finer-resolution simulations is attributed to decreases in slope and curvature of the underlying DEM and is consistent with the findings of other studies (Kuo, 1999; Niedda, 2004).

We analyzed the loss of variance due to coarsening of the DEM using information theory (Shannon and Weaver, 1949). The information content, I, a measure of the variability of a parameter, is defined as

$$I = -\sum_{j=1}^{N} p_j \ln(p_j) \tag{7}$$

HESSD
11, 12833–12882, 2014

where N is the number of bins into which the parameter range is divided and p_j is the proportion of the parameter in the jth bin. The information content for slope and curvature decreased with coarser grids for all four study sites (Fig. 7). Similar to results reported by Kuo (1999), our study site had a larger decrease in I with increasing grid resolution for curvature than slope. Both, slope and curvature of the terrain contribute to prediction of mean soil moisture via governing equations of subsurface flow, thus a loss in I with increasing grid size implies that the hydrologic response of the model will be less spatially variable at coarser resolution.

We aggregated the simulated θ at 0.25, 2, and 8 m resolutions (Fig. 6) and then computed variance for the coarsened soil moisture predictions. Each successive coarsening of the soil moisture field led to a decrease in variance, but these decreases are not as large as those calculated from the model simulations at the coarser resolutions. This result shows non-linear impacts of DEM resolution on simulated soil moisture. As in many observational (Teuling and Troch, 2005; Brocca et al., 2010) and modeling (Albertson and Montaldo, 2003) studies of temperate watersheds, our model predictions for the four polygonal tundra sites resulted in a concave-up relationship between variance and mean soil moisture (Fig. 8). At low (high) $\overline{\theta}$, soil moisture variance is expected to be low since the entire domain is expected to be relatively dry (wet). At an intermediate mean moisture value, soil moisture variance reached a peak value, $\sigma^2_{\theta,\,\mathrm{peak}}$, that differed between sites. The framework presented by Yeh and Eltahir (1998) to describe the relationship between topography and spatial distribution of soil moisture explains the variation of simulated σ^2_θ across our study sites. Yeh and Eltahir (1998) showed that for a steady state assumption and when only accounting for variability in surface topography, σ^2_θ is a linear function of the variance in elevation, σ^2_z (Eq. 20 of Yeh and Eltahir, 1998). In order to investigate the σ^2_θ–σ^2_z relationship at our Barrow sites, we created seven mean soil moisture bins between 0.52–0.58; for each study site, the mean σ^2_θ for each soil moisture bin is computed (Fig. 11). Simulated soil moisture variance is largest for sites B and C, which have the highest σ^2_z; followed by sites A and D, respectively, which agrees with results presented in Yeh and Eltahir (1998). The slope of the linear

σ_θ^2–σ_z^2 relationship exhibits a non-linear relationship with $\overline{\theta}$ (Fig. 10), which similar to the σ_θ^2–$\overline{\theta}$ relationship. This analysis shows that the steady state linear relationship between soil moisture variance and topography as suggested by Yeh and Eltahir (1998) is applicable in the transient case with the modification that slope of σ_θ^2–σ_z^2 is dependent on transient mean soil moisture.

Ivanov et al. (2010) reported hysteresis between C_v and $\overline{\theta}$ for a steep zero-order basin in a semiarid climate. The design of numerical experiments by Ivanov et al. (2010) ensured an absence of infiltration excess runoff generation and topography induced subsurface soil moisture redistribution was attributed as the chief cause of the non-unique relationship between C_v and $\overline{\theta}$. In our study sites, the presence of polygonal surface features created preferential flow and infiltration pathways for surface flows, which resulted in an overall increase in σ_θ^2 after rainfall events and resulted in an absence of hysteretic relationships between C_v and $\overline{\theta}$.

Next we examine relationships between simulated soil moisture variance and spatial resolution at all sites for the entire simulation period. To illustrate the patterns that emerged, we discuss these relationships at Site A for the driest (t = 71 day) and wettest (t = 84 day) conditions (Fig. 11). Also shown are soil moisture variance estimated by aggregating the finest-resolution simulation across spatial resolutions for the same two days. It is evident from Fig. 11 that soil moisture variance exhibits non-linear scaling, as has been observed in many previous studies (Nykanen and Foufoula-Georgiou, 2001; Lawrence and Hornberger, 2007; Brocca et al., 2012).

3.2 Estimation of fine-resolution soil moisture PDF

In this polygonal tundra system the soil moisture distribution is strongly controlled by topography, exhibiting a strong inverse relationship between saturation and elevation (Fig. 12). We therefore investigated an approach to estimate both the full probability distribution function (PDF) of fine-resolution soil moisture (with $f_\Theta(\theta)$ representing the PDF from the fine-resolution simulations) and its moments using coarse-resolution simulations and site-level topography. We developed an estimated soil moisture PDF ($f_\Theta(\theta)$) by rotating the probability distribution function of the DEM, $f_Z(z)$, about its mean and scaling the rotated $f_Z(z)$ by the predicted coarse-resolution maximum ($\theta^{\text{fine}}_{\text{max}}$) and minimum ($\theta^{\text{fine}}_{\text{min}}$) soil moisture at the finest resolution for each day. $\theta^{\text{fine}}_{\text{max}}$ and $\theta^{\text{fine}}_{\text{min}}$ are obtained from coarse-resolution mean soil moisture ($\overline{\theta}$) simulations using a best-fit cubic polynomial curve:

$$\theta^{\text{fine}}_{\text{max/min}} = \gamma_3 \overline{\theta}^3 + \gamma_2 \overline{\theta}^2 + \gamma_1 \overline{\theta} + \gamma_0 \quad (8)$$

where γ_i are best-fit coefficients. The estimated (from Eq. (10) and the coarse-resolution simulations) and fine-resolution simulated $f_\Theta(\theta)$ showed very good correspondence (e.g., Fig. 13 for Site A). The agreement between estimated and simulated fine-resolution PDF is better for drier conditions than wetter conditions, and the estimated PDF underestimates soil moisture at higher $\overline{\theta}$ conditions. The ability to predict the soil moisture PDF from the inverted and scaled DEM PDF is consistent with the idea that, in polygonal tundra, the relatively lower elevations (troughs) are more likely to be saturated, the relatively higher elevations (rims) are less likely to be saturated, and there is a dominant PDF peak at an intermediate soil moisture corresponding to the polygon centers (which have the largest fractional cover in the polygons). The close correspondence between simulated and inferred soil moisture PDFs using the transformed elevation PDF in each site provides a quantitative method to estimate moisture over time that qualitatively matches this intuitively reasonable distribution.

We next compared the first four central moments from the estimated (Eq. 10) and simulated PDFs (e.g., Fig. 14 for Site A). The bias and correlation of the first four central moments across all four sites are $< \pm 4\,\%$ and > 0.99, respectively (Table 4). Although these estimated moments are of comparable accuracy to those developed by relating the moments to the mean moisture field (Sect. 3.2), the ability to predict the full PDF provides a potentially more accurate representation of the dynamically varying soil moisture field.

HESSD
11, 12833–12882, 2014

Title Page
Abstract | Introduction
Conclusions | References
Tables | Figures
◄| |►
◄ ►
Back | Close
Full Screen / Esc
Printer-friendly Version
Interactive Discussion

3.3 Estimation of fine scale soil moisture field

The approach presented in the previous section estimated statistical properties of the soil moisture distribution at finer spatial resolution from coarse resolution simulations without explicitly retrieving θ at fine resolution. In this section, we present two approaches to downscale simulated coarse-resolution soil moisture fields to estimate fine-resolution soil moisture. The first downscaling approach uses soil moisture simulations results at both fine and coarse resolution to develop spatially-explicit, time-varying downscaling factors. The second downscaling approach estimates spatially-explicit time-invariant factors based on elevation at fine and coarse resolutions. In the first downscaling approach, for a given fine-grid cell (i,j), daily downscaling factors, d_θ, to map soil moisture from 8 to 0.25 m is computed as:

$$d_\theta(i,j,t) = \frac{\theta_{0.25\,\mathrm{m}}(i,j,t)}{\theta_{8\,\mathrm{m}}(i^*,j^*,t)} \tag{9}$$

where $\theta_{0.25\,\mathrm{m}}$ and $\theta_{8\,\mathrm{m}}$ are simulated soil moisture at 0.25 and 8 m, respectively, and (i^*,j^*) is the corresponding coarse resolution grid cell that encompasses the fine grid cell. The temporally averaged downscaling factor, $\overline{d_\theta}$, is less than 1.0 for rims of high centered-polygons (in Site A and C) and centers of high-centered polygons (in Site B and C); while centers and troughs of low-centered polygons had values of $\overline{d_\theta}$, > 1. (Fig. 15). The downscaling factor for Site D had an overall value greater than 1.0 without a dominant spatial pattern of $\overline{d_\theta}$ in comparison to the other three sites because of an absence of troughs at Site D (Table 1). The estimated d_θ map showed imprints of a coarse grid cell for certain portions of the domain (Fig. 15a). In order to capture the temporal variation in the downscaling factor, we fitted the following linear regression to relate the downscaling factor for each fine grid cell with the simulated coarse resolution soil moisture:

$$d_\theta(i,j,t) = \lambda_1\theta_{8\,\mathrm{m}}(i^*,j^*,t) + \lambda_0 \tag{10}$$

HESSD
11, 12833–12882, 2014

where λ_0 and λ_1 are best-fit coefficients. Daily absolute relative error in soil moisture, $\varepsilon(d_\theta)$, is computed between the estimated, $\theta^{d_\theta}_{0.25\,\mathrm{m}}$, and simulated, $\theta_{0.25\,\mathrm{m}}$, values at the fine-resolution as:

$$\varepsilon(d_\theta) = \left| \frac{\theta^{d_\theta}_{0.25\,\mathrm{m}} - \theta_{0.25\,\mathrm{m}}}{\theta_{0.25\,\mathrm{m}}} \right| \times 100 \tag{11}$$

The maximum and mean $\varepsilon(d_\theta)$ for all study sites are $< \pm 0.34$ and $< \pm 0.03\,\%$, respectively (Table 5). Additionally, we used a temporally averaged downscaling factor to estimate daily fine-scale soil moisture fields; maximum and mean $\varepsilon(\overline{d_\theta})$ are $< \pm 3.78$ and $< \pm 0.16\,\%$, respectively.

With the demonstrated success of $\overline{d_\theta}$ in estimating fine-scale soil moisture from coarse resolution simulations, we developed a second downscaling approach by relating the mean soil moisture downscaling factor with the DEM. Downscaling factors are computed using the same approach as for d_θ for three DEM characteristics: elevation (d_e), slope (d_s), and curvature (d_c) for each study site. A pair-wise linear regression analysis between d_θ and the three DEM characteristics showed an existence of a strong linear relationship between d_θ and d_e (Fig. 16), while a linear relationship is not found between d_θ–d_S and d_θ–d_C. We next estimated daily snapshots of fine-resolution soil moisture based on d_θ obtained from linear relationship of d_e (Fig. 17). The maximum and mean error in estimated soil moisture using d_θ based on DEM characteristics for all study sites are $< \pm 5.24$ and $< \pm 0.88\,\%$, respectively (Table 5).

Even though both downscaling approaches can accurately capture spatial distributions of soil moisture at the finest resolution (with mean error $< \pm 1\,\%$), the first downscaling method is able to accurately preserve fine-scale soil moisture variance for all study sites, while second downscale method significantly underestimates σ^2_θ (Fig. 18). Additionally, the first downscaling method is able to reproduce scaling behavior of soil moisture variance as obtained by fine-scale simulation, while the second method underestimates this relationship. The reason for the failure of the second downscaling

HESSD
11, 12833–12882, 2014

Topographic controls on soil moisture scaling properties

G. Bisht and W. J. Riley

approach can be explained on the basis of the $\overline{\theta}$–σ_θ^2 relationships. It is evident from Fig. 8 that mean and variance of soil moisture exhibit a non-monotonic relationship and use of time-invariant downscaling factors is unable to capture the non-monotonicity of the $\overline{\theta}$–σ_θ^2 relationship. Additionally, the first downscaling approach is able to more accurately estimate soil moisture variance as a function of resolution (Fig. 19). While the second downscaling method has the advantage of relying solely on fine- and coarse-resolution elevation, it is less accurate in estimating soil moisture variance at finer resolution. Future studies will attempt to develop the $\overline{\theta}$–σ_θ^2 solely based on DEM characteristics at the two resolutions.

3.4 Impact of vegetation heterogeneity of fine scale soil moisture simulation

The results presented in previous Sects. 3.1–3.4 assumed no heterogeneity in vegetation cover and applied a horizontally homogenous evapotranspiration sink within the subsurface domain of PFLOTRAN model. As reported by Gangodagamage et al. (2014), our study site has varying vegetation types that are associated polygonal landscape features: mosses and sedges are mostly present in wetter parts of the domain (troughs and centers of low-centered polygons); while lichen and shrubs mainly cover drier areas (rims of low-centered polygons and centers of high-centered polygons). As a first step to account for vegetation heterogeneity, we spatially varied the evapotranspiration sink based on the vegetation distribution. Based on the scaling factor (Sect. 3.3; Fig. 15), the evapotranspiration sink was increased (decreased) by 50 % for regions with d_θ greater (less) than 1. A set of additional PFLOTRAN simulations was performed with modified ET for all four sites at 0.25 [m]. Soil moisture variance with and without vegetation heterogeneity did not show any appreciable differences across all four sites (Fig. 20). The lack of contrast within the simulation results when heterogeneous vegetation cover was accounted for may be attributed to several reasons: (1) evapotranspiration sinks in the high Arctic are low, (2) the imposed simple

HESSD
11, 12833–12882, 2014

vegetation cover (50 % higher or lower ET) oversimplified the natural system, and (3) soil moisture-vegetation feedbacks were not accounted for.

4 Summary and conclusions

In this study, we analyzed multi-year surface–subsurface isothermal flow simulations during summer months for four polygonal ground study sites near Barrow, AK. PFLOTRAN simulations are performed at six different spatial resolutions for each of the four study sites. We analyzed simulation results to characterize spatial scaling of statistical moments for soil moisture and developed relationships to predict those statistical moments at fine-resolution from coarse-resolution simulations. Although coarse-resolution simulations are able to accurately represent mean soil moisture, soil moisture variance is significantly under estimated in coarser-resolution simulations. Soil moisture variance decreased at coarser resolution due to loss of information content of slope and curvature of the underlying DEM. However, the observed decrease in soil moisture variance in coarser-resolution simulations is greater than the decrease in soil moisture variance obtained by coarsening out the fine-resolution simulation.

A concave relationship between soil moisture mean and variance without a hysteresis effect is predicted. The PDF of topography and soil moisture are strongly inversely correlated and a method to obtain the fine-resolution soil moisture PDF from coarse-resolution simulations is developed and tested. The inferred soil moisture PDF accurately represented the fine-resolution simulated PDF. The moments computed from the inferred soil moisture PDF were in very good agreement when compared to moments derived from fine-resolution simulations.

Several important caveats need to be acknowledged regarding our results. Our simulations assumed a static active layer depth corresponding approximately to the maximum seasonal value seen at the NGEE-Arctic sites. Although we included a first-order estimate of vertical heterogeneity in soil types, horizontal heterogeneity and vertical heterogeneity associated with cryoturbative mixing were neglected. The evapotranspi-

HESSD
11, 12833–12882, 2014

ration flux is prescribed from an offline CLM simulation, implying that we were unable to account for soil moisture-ET feedbacks and horizontal heterogeneity in vegetation type. Although we believe that our basic conclusions regarding polygonal tundra soil moisture spatial structure and topographic controls are valid, future work should characterize the impacts of these simplifications on our conclusions.

Finally, though the method to estimate the soil moisture probability density function from coarse-resolution simulations is accurate, that method is unable to retrieve the spatially explicit dynamic fine-resolution soil moisture field. We therefore presented two methods to map simulated coarse resolution soil moisture data onto fine resolution grid using downscaling factors. The first downscaling approach, based on fine- and coarse-resolution simulations, is able to capture mean and variance of soil moisture at fine resolution. The second downscaling approach, which relied only on DEMs at the two resolutions, is able to capture spatial pattern θ, but underestimates soil moisture variance. We are presently exploring additional methods to infer the spatial structure of soil moisture at fine resolution from coarse-resolution simulations using a Principal Orthogonal Decomposition method (Pau et al., 2014). The ultimate goal of using fine-resolution simulations to improve prediction of coarse-resolution hydrological and biogeochemical exchanges with the atmosphere requires further work to develop fine-resolution models of representative landscapes, develop ROMs from these models, and integrate those ROMs into a coarser-resolution land model. We believe such an approach is a viable method to represent fine-resolution heterogeneity in climate-scale land models.

Acknowledgements. This research is conducted under the Next-Generation Ecosystem Experiments (NGEE Arctic) project supported by the Office of Biological and Environmental Research in the DOE Office of Science, through Contract No. DE-AC02-05CH11231 between Lawrence Berkeley National Laboratory and the US Department of Energy.

References

Albertson, J. D. and Montaldo, N.: Temporal dynamics of soil moisture variability: 1. Theoretical basis, Water Resour. Res., 39, 1274, doi:10.1029/2002WR001616, 2003.

Balay, S., Brown, J., Buschelman, K., Gropp, W. D., Kaushik, D., Knepley, M. G., McInnes, L. C., Smith, B. F., and Zhang, H.: PETSc Users Manual, Argonne National Laboratory, 2013.

Bockheim, J. G.: Importance of cryoturbation in redistributing organic carbon in permafrost-affected soils, Soil Sci. Soc. Am. J., 71, 1335–1342, doi:10.2136/sssaj2006.0414N, 2007.

Bridgham, S. D., Updegraff, K., and Pastor, J.: Carbon, nitrogen, and phosphorous mineralization in northern wetlands, Ecology, 79, 1545–1561, doi:10.1890/0012-9658(1998)079[1545:CNAPMI]2.0.CO;2, 1998.

Brocca, L., Melone, F., Moramarco, T., and Morbidelli, R.: Spatial–temporal variability of soil moisture and its estimation across scales, Water Resour. Res., 46, W02516, doi:10.1029/2009WR008016, 2010.

Brocca, L., Tullo, T., Melone, F., Moramarco, T., and Morbidelli, R.: Catchment scale soil moisture spatial–temporal variability, J. Hydrol., 422–423, 63–75, doi:10.1016/j.jhydrol.2011.12.039, 2012.

Chapin III, F. S., Matson, P. A., and Mooney, H. A.: Principles of Terrestrial Ecosystem Ecology, Springer, New York, 2002.

Childs, E. C.: The use of soil moisture characteristics in soil studies, Soil Sci., 50, 239–252, 1940.

Choi, H., Kumar, P., and Liang, X.-Z.: Three-dimensional volume-averaged soil moisture transport model with a scalable parameterization of subgrid topographic variability, Water Resour. Res., 43, W04414, doi:10.1029/2006WR005134, 2007.

Choi, M. and Jacobs, J. M.: Spatial soil moisture scaling structure during Soil Moisture Experiment 2005, Hydrol. Process., 25, 926–932, doi:10.1002/hyp.7877, 2011.

Dubayah, R., Wood, E. F., and Lavallee, D.: Multiscaling analysis in distributed modeling and remote sensing: an application using soil moisture, in: Scale in Remote Sensing and GIS, edited by: Quattrochi, D. A. and Goodchild, M. F., CRC Lewis, Boca Raton, FL, 93–112, 1997.

Engstrom, R., Hope, A., Kwon, H., Stow, D., and Zamolodchikov, D.: Spatial distribution of near surface soil moisture and its relationship to microtopography in the Alaskan Arctic coastal plain, Nord. Hydrol., 36, 219–234, 2005.

Famiglietti, J. S., Devereaux, J. A., Laymon, C. A., Tsegaye, T., Houser, P. R., Jackson, T. J., Graham, S. T., Rodell, M., and van Oevelen, P. J.: Ground-based investigation of soil moisture variability within remote sensing footprints during the southern Great Plains 1997 (SGP97) Hydrology Experiment, Water Resour. Res., 35, 1839–1851, doi:10.1029/1999WR900047, 1999.

Famiglietti, J. S., Ryu, D., Berg, A. A., Rodell, M., and Jackson, T. J.: Field observations of soil moisture variability across scales, Water Resour. Res., 44, W01423, doi:10.1029/2006WR005804, 2008.

Gangodagamage, C., Rowland, J. C., Hubbard, S. S., Brumby, S. P., Liljedahl, A. K., Wainwright, H., Wilson, C. J., Altmann, G. L., Dafflon, B., Peterson, J., Ulrich, C., Tweedie, C. E., and Wullschleger, S. D.: Extrapolating active layer thickness measurements across Arctic polygonal terrain using LiDAR and NDVI data sets, Water Resour. Res., 50, 6339–6357, doi:10.1002/2013WR014283, 2014.

Gebremichael, M., Rigon, R., Bertoldi, G., and Over, T. M.: On the scaling characteristics of observed and simulated spatial soil moisture fields, Nonlin. Processes Geophys., 16, 141–150, doi::10.5194/npg-16-141-2009, 2009.

Hammond, G. E., Lichtner, P. C., Lu, C., and Mills, R. T.: PFLOTRAN: reactive flow and transport code for use on laptops to leadership-class supercomputers, in: Groundwater Reactive Transport Models edited by: Zhang, F., Yeh, G. T., and Parker, J. C., Bentham Science Publishers, Sharjah, UAE,141–159, 2012.

Hinkel, K. M., Eisner, W. R., Bockheim, J. G., Nelson, F. E., Peterson, K. M., and Dai, X.: Spatial extent, age, and carbon stocks in drained thaw lake basins on the Barrow Peninsula, Alaska, Arct. Antarct. Alp. Res., 35, 291–300, doi:10.1657/1523-0430(2003)035[0291:SEAACS]2.0.CO;2, 2003.

Hinkel, K. M., Frohn, R. C., Nelson, F. E., Eisner, W. R., and Beck, R. A.: Morphometric and spatial analysis of thaw lakes and drained thaw lake basins in the western Arctic Coastal Plain, Alaska, Permafrost Periglac., 16, 327–341, doi:10.1002/ppp.532, 2005.

Hinkel, K. M., Jones, B. M., Eisner, W. R., Cuomo, C. J., Beck, R. A., and Frohn, R.: Methods to assess natural and anthropogenic thaw lake drainage on the western Arctic coastal plain of northern Alaska, J. Geophys. Res.-Earth, 112, F02S16, doi:10.1029/2006JF000584, 2007.

Hinzman, L. D. and Kane, D. L.: Potential repsonse of an Arctic watershed during a period of global warming, J. Geophys. Res.-Atmos., 97, 2811–2820, doi:10.1029/91JD01752, 1992.

Hinzman, L. D., Kane, D. L., Benson, C. S., and Everett, K. R.: Hydrologic and thermal properties of the active layer in the Alaskan Arctic, Cold Reg. Sci. Technol., 19, 95–110, 1991.
Holland, M. M. and Bitz, C. M.: Polar amplification of climate change in coupled models, Clim. Dynam., 21, 221–232, doi:10.1007/s00382-003-0332-6, 2003.
Hu, Z., Islam, S., and Cheng, Y.: Statistical characterization of remotely sensed soil moisture images, Remote Sens. Environ., 61, 310–318, doi:10.1016/S0034-4257(97)89498-9, 1997.
Ivanov, V. Y., Fatichi, S., Jenerette, G. D., Espeleta, J. F., Troch, P. A., and Huxman, T. E.: Hysteresis of soil moisture spatial heterogeneity and the "homogenizing" effect of vegetation, Water Resour. Res., 46, W09521, doi:10.1029/2009WR008611, 2010.
Jana, R. B. and Mohanty, B. P.: On topographic controls of soil hydraulic parameter scaling at hillslope scales, Water Resour. Res., 48, W02518, doi:10.1029/2011wr011204, 2012a.
Jana, R. B. and Mohanty, B. P.: A topography-based scaling algorithm for soil hydraulic parameters at hillslope scales: field testing, Water Resour. Res., 48, W02519, doi:10.1029/2011WR011205, 2012b.
Jorgenson, M. T., Shur, Y. L., and Pullman, E. R.: Abrupt increase in permafrost degradation in Arctic Alaska, Geophys. Res. Lett., 33, L02503, doi:10.1029/2005GL024960, 2006.
Koven, C., Friedlingstein, P., Ciais, P., Khvorostyanov, D., Krinner, G., and Tarnocai, C.: On the formation of high-latitude soil carbon stocks: effects of cryoturbation and insulation by organic matter in a land surface model, Geophys. Res. Lett., 36, L21501, doi:10.1029/2009GL040150, 2009.
Koven, C. D., Ringeval, B., Friedlingstein, P., Ciais, P., Cadule, P., Khvorostyanov, D., Krinner, G., and Tarnocai, C.: Permafrost carbon-climate feedbacks accelerate global warming, P. Natl. Acad. Sci. USA, 108, 14769–14774, doi:10.1073/pnas.1103910108, 2011.
Kumar, P.: Layer averaged Richard's equation with lateral flow, Adv. Water Resour., 27, 521–531, doi:10.1016/j.advwatres.2004.02.007, 2004.
Lawrence, J. E. and Hornberger, G. M.: Soil moisture variability across climate zones, Geophys. Res. Lett., 34, L20402, doi:10.1029/2007GL031382, 2007.
Li, B. and Rodell, M.: Spatial variability and its scale dependency of observed and modeled soil moisture over different climate regions, Hydrol. Earth Syst. Sci., 17, 1177–1188, doi:10.5194/hess-17-1177-2013, 2013.
Liljedahl, A. K., Hinzman, L. D., Harazono, Y., Zona, D., Tweedie, C. E., Hollister, R. D., Engstrom, R., and Oechel, W. C.: Nonlinear controls on evapotranspiration in arctic coastal wetlands, Biogeosciences, 8, 3375–3389, doi:10.5194/bg-8-3375-2011, 2011.

Manning, R.: On the flow of water in open channels and pipes, Transactions of the Institution of Civil Engineers of Ireland, 20, 161–207, 1891.
McFadden, J. P., Chapin, F. S., and Hollinger, D. Y.: Subgrid-scale variability in the surface energy balance of arctic tundra, J. Geophys. Res.-Atmos., 103, 28947–28961, doi:10.1029/98JD02400, 1998.
McGuire, A. D., Clein, J. S., Melillo, J. M., Kicklighter, D. W., Meier, R. A., Vorosmarty, C. J., and Serreze, M. C.: Modelling carbon responses of tundra ecosystems to historical and projected climate: sensitivity of pan-Arctic carbon storage to temporal and spatial variation in climate, Glob. Change Biol., 6, 141–159, doi:10.1046/j.1365-2486.2000.06017.x, 2000.
Miller, P. C., Stoner, W. A., and Tieszen, L. L.: A model of stand photosynthesis for the wet meadow tundra at Barrow, Alaska, Ecology, 57, 411–430, doi:10.2307/1936428, 1976.
Minke, M., Donner, N., Karpov, N., de Klerk, P., and Joosten, H.: Patterns in vegetation composition, surface height and thaw depth in polygon mires in the Yakutian Arctic (NE Siberia): a microtopographical characterisation of the active layer, Permafrost Periglac., 20, 357–368, doi:10.1002/ppp.663, 2009.
Nykanen, D. K. and Foufoula-Georgiou, E.: Soil moisture variability and scale-dependency of nonlinear parameterizations in coupled land–atmosphere models, Adv. Water Resour., 24, 1143–1157, doi:10.1016/S0309-1708(01)00046-X, 2001.
Oberbauer, S. F., Tenhunen, J. D., and Reynolds, J. F.: Environmental effects on CO_2 efflux from water track and Tussock Tundra in Arctic Alaska, USA, Arctic Alpine Res., 23, 162–169, doi:10.2307/1551380, 1991.
Oechel, W. C., Hastings, S. J., Vourlrtis, G., Jenkins, M., Riechers, G., and Grulke, N.: Recent change of Arctic tundra ecosystems from a net carbon dioxide sink to a source, Nature, 361, 520–523, doi:10.1038/361520a0, 1993.
Oleson, K. W., Lawrence, D. M., Bonan, G. B., Drewniak, B., Huang, M., Koven, C. D., Levis, S., Li, F., Riley, W. J., Subin, Z. M., Swenson, S. C., Thornton, P. E., Bozbiyik, A., Fisher, R., Kluzek, E., Lamarque, J.-F., Lawrence, P. J., Leung, L. R., Lipscomb, W., Muszala, S., Ricciuto, D. M., Sacks, W., Sun, Y., Tang, J., and Yang, Z.-L.: Technical Description of Version 4.5 of the Community Land Model (CLM), National Center for Atmospheric Research, Boulder, CO, 2013.
Pau, G. S. H., Bisht, G., and Riley, W. J.: A reduced order modeling approach to represent subgrid-scale hydrological dynamics for regional- and climate-scale land-surface simulations:

application in a polygonal tundra landscape, Geosci. Model Dev. Discuss., 7, 2125-2172, doi:10.5194/gmdd-7-2125-2014, 2014.

Quinton, W. L. and Marsh, P.: The influence of mineral earth hummocks on subsurface drainage in the continuous permafrost zone, Permafrost Periglac., 9, 213–228, 1998.

Riley, W. J. and Shen, C.: Characterizing coarse-resolution watershed soil moisture heterogeneity using fine-scale simulations, Hydrol. Earth Syst. Sci., 18, 2463–2483, doi:10.5194/hess-18-2463-2014, 2014.

Riordan, B., Verbyla, D., and McGuire, A. D.: Shrinking ponds in subarctic Alaska based on 1950–2002 remotely sensed images, J. Geophys. Res.-Biogeo., 111, G04002, doi:10.1029/2005JG000150, 2006.

Rodriguez-Iturbe, I., Vogel, G. K., Rigon, R., Entekhabi, D., Castelli, F., and Rinaldo, A.: On the spatial organization of soil moisture fields, Geophys. Res. Lett., 22, 2757–2760, doi:10.1029/95GL02779, 1995.

Schaefer, K., Zhang, T., Bruhwiler, L., and Barrett, A. P.: Amount and timing of permafrost carbon release in response to climate warming, Tellus B, 63, 165–180, doi:10.1111/j.1600-0889.2011.00527.x, 2011.

Schuur, E. A. G., Bockheim, J., Canadell, J. G., Euskirchen, E., Field, C. B., Goryachkin, S. V., Hagemann, S., Kuhry, P., Lafleur, P. M., Lee, H., Mazhitova, G., Nelson, F. E., Rinke, A., Romanovsky, V. E., Shiklomanov, N., Tarnocai, C., Venevsky, S., Vogel, J. G., and Zimov, S. A.: Vulnerability of permafrost carbon to climate change: implications for the global carbon cycle, Bioscience, 58, 701–714, doi:10.1641/B580807, 2008.

Schuur, E. A. G. and Abbott, B.: Climate change: high risk of permafrost thaw, Nature, 480, 32–33, 2011.

Seppala, M., Gray, J., and Ricard, J.: Development of low–centred ice–wedge polygons in the northernmost Ungava Peninsual, Queébec, Canada, Boreas, 20, 259–285, doi:10.1111/j.1502-3885.1991.tb00155.x, 1991.

Sivapalan, M. and Woods, R. A.: Evaluation of the effects of general circulation models' subgrid variability and patchiness of rainfall and soil moisture on land surface water balance fluxes, Hydrol. Process., 9, 697–717, doi:10.1002/hyp.3360090515, 1995.

Stocker, T. F., Qin, D., Plattner, G.-K., Tignor, M., Allen, S. K., Boschung, J., Nauels, A., Xia, Y., Bex, V., and Midgley, P. M.: IPCC, 2013: summary for policymakers, in: Climate Change 2013: The Physical Science Basis, Contribution of Working Group I to the Fifth Assessment

HESSD
11, 12833–12882, 2014

Report of the Intergovernmental Panel on Climate Change, Cambridge University Press, Cambridge, UK and New York, USA, 1535 pp., 2013.
Tarnocai, C., Canadell, J. G., Schuur, E. A. G., Kuhry, P., Mazhitova, G., and Zimov, S.: Soil organic carbon pools in the northern circumpolar permafrost region, Global Biogeochem. Cy., 23, GB2023, doi:10.1029/2008GB003327, 2009.
Teuling, A. J. and Troch, P. A.: Improved understanding of soil moisture variability dynamics, Geophys. Res. Lett., 32, L05404, doi:10.1029/2004GL021935, 2005.
Torn, M. S. and Chapin Iii, F. S.: Environmental and biotic controls over methane flux from Arctic tundra, Chemosphere, 26, 357–368, doi:10.1016/0045-6535(93)90431-4, 1993.
van Genuchten, M. T.: A closed-form equation for predicting the hydraulic conductivity of unsaturated soils, Soil Sci. Soc. Am. J., 44, 892–898, doi:10.2136/sssaj1980.03615995004400050002x, 1980.
Wiggins, I. L.: The distribution of vascular plants on polygonal ground near Point Barrow, Alaska, in: Stanford University Contributions of the Dudley Herbarium, Natural History Museum of Stanford University, Stanford, 4, 41–52, 1951.
Williams, T. and Flanagan, L.: Effect of changes in water content on photosynthesis, transpiration and discrimination against 13CO2 and C18O16O in Pleurozium and Sphagnum, Oecologia, 108, 38–46, doi:10.1007/BF00333212, 1996.
Yeh, P. J. F. and Eltahir, E. A. B.: Stochastic analysis of the relationship between topography and the spatial distribution of soil moisture, Water Resour. Res., 34, 1251–1263, doi:10.1029/98WR00093, 1998.
Zona, D., Lipson, D. A., Zulueta, R. C., Oberbauer, S. F., and Oechel, W. C.: Microtopographic controls on ecosystem functioning in the Arctic Coastal Plain, J. Geophys. Res.-Biogeo., 116, G00I08, doi:10.1029/2009JG001241, 2011.

HESSD
11, 12833–12882, 2014

Topographic controls on soil moisture scaling properties

G. Bisht and W. J. Riley

Table 1. Characteristics of NGEE-Arctic study sites.

Site	Polygonal characteristics	Mean elevation [m]	Standard deviation of elevation [m]
A	Low centered polygons with troughs	4.66	0.10
B	High centered polygons	4.68	0.12
C	Transitional polygons	4.44	0.12
D	Low centered polygons without troughs	4.27	0.07

HESSD
11, 12833–12882, 2014

HESSD
11, 12833–12882, 2014

Topographic controls on soil moisture scaling properties

G. Bisht and W. J. Riley

Table 2. van Genuchten model parameters used to fit data reported in Hinzman et al. (1991).

	0–5 cm	5–10 cm	20–25 cm
θ_s [m^3 m^{-3}]	0.9	0.86	0.55
θ_r [m^3 m^{-3}]	0.05	0.05	0.05
α [m^{-1}]	2.0	1.0	1.5
K_{sat} [cm min^{-1}]	1.1640	0.6240	0.0564
n [–]	1.35	1.35	1.25

Table 3. Bias and correlation (R^2) for soil moisture moments computed from PFLTORAN simulations at multiple resolutions and cubic polynomial curve relationship (described in Sect. 3.2).

	2nd Central Moment		3rdCentral Moment		4th Central Moment	
	Bias	R^2	Bias	R^2	Bias	R^2
A	−0.03 %	0.999	0.52 %	0.999	−0.14 %	0.997
B	−0.08 %	0.997	−3.04 %	0.998	−0.35 %	0.996
C	−0.08 %	0.993	−0.94 %	0.994	−0.33 %	0.989
D	−0.26 %	0.982	−0.55 %	0.976	0.07 %	0.974

HESSD
11, 12833–12882, 2014

Table 4. Bias and correlation (R^2) for moments computed from the soil moisture probability density function based on fine-resolution simulations and estimated PDF from coarse-resolution simulations (described in Sect. 3.2).

	1st Moment		2nd Central Moment		3rd Central Moment		4th Central Moment	
	Bias	R^2	Bias	R^2	Bias	R^2	Bias	R^2
A	1.43 %	0.996	1.80 %	0.996	2.19 %	0.995	2.58 %	0.994
B	1.73 %	0.996	2.42 %	0.996	3.12 %	0.995	3.82 %	0.994
C	0.31 %	0.994	−0.44 %	0.993	−1.18 %	0.993	−1.93 %	0.992
D	0.72 %	0.999	0.42 %	0.999	0.12 %	0.999	−0.17 %	0.998

HESSD
11, 12833–12882, 2014

Table 5. Maximum and mean absolute error between simulated soil moisture field at 0.25 m and estimated soil moisture based on three types of downscaling factors.

Downscaling factor			A	B	C	D
Based on	Temporal resolution					
Simulation	Varying in time	Maximum error	0.23 %	0.34 %	0.28 %	0.16 %
		Mean error	0.02 %	0.02 %	0.03 %	0.01 %
Simulation	Constant in time	Maximum error	2.40 %	2.19 %	3.78 %	2.57 %
		Mean error	0.12 %	0.16 %	0.12 %	0.08 %
DEM	Constant in time	Maximum error	3.23 %	5.24 %	4.50 %	3.30 %
		Mean error	0.65 %	0.88 %	0.61 %	0.28 %

HESSD
11, 12833–12882, 2014

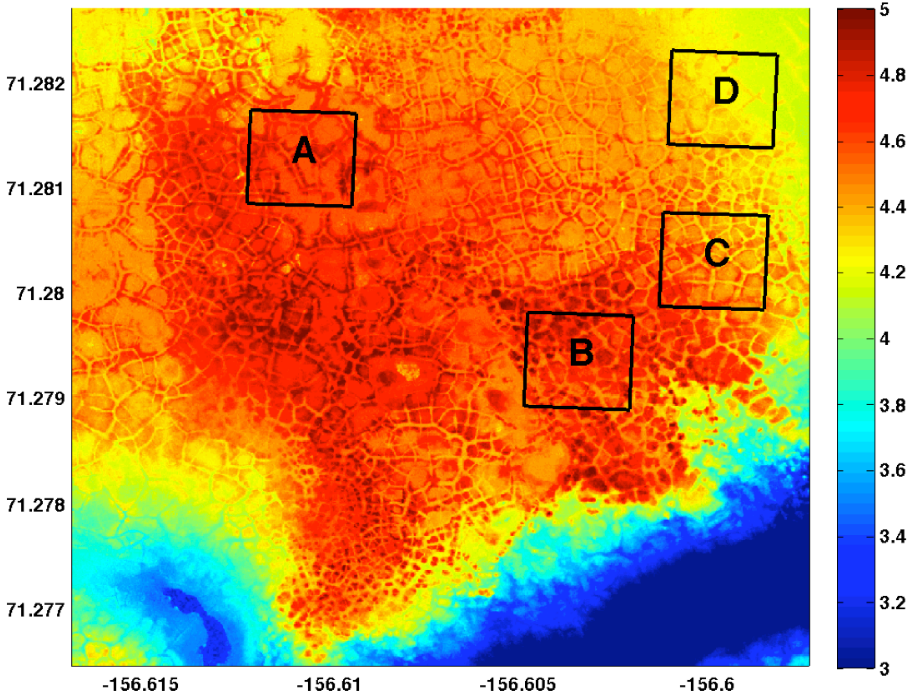

Figure 1. LIDAR DEM for the four NGEE-Arctic study sites.

HESSD
11, 12833–12882, 2014

Topographic controls on soil moisture scaling properties

G. Bisht and W. J. Riley

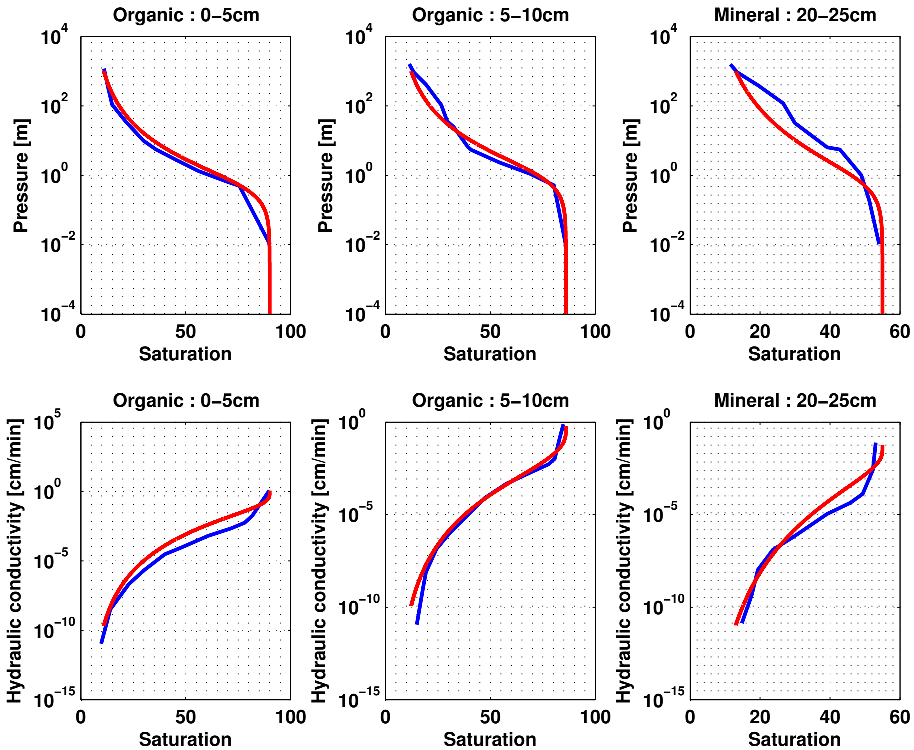

Figure 2. Fitted van Genuchten model (in red) to data (in blue) reported in Hinzman et al. (1991).

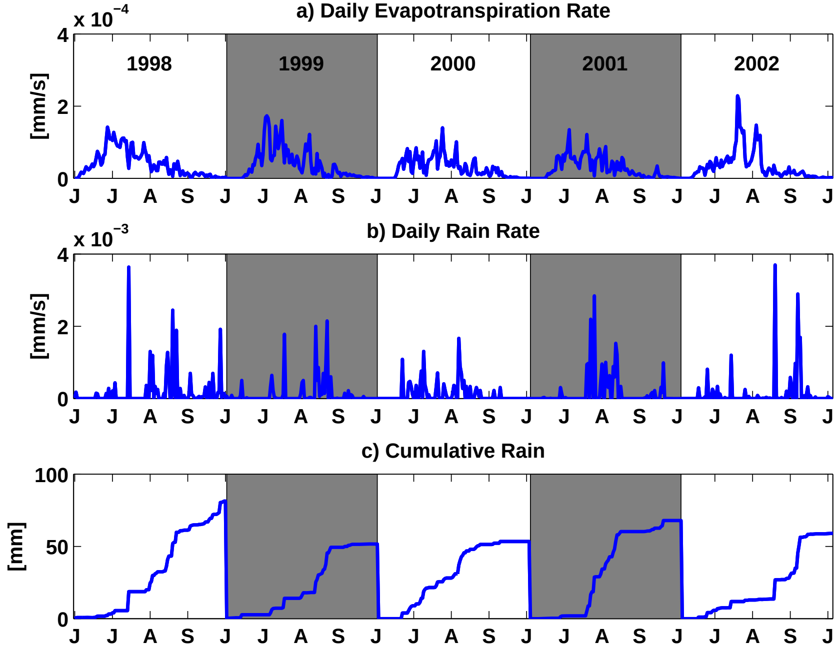

Figure 3. Time series of meteorological forcing dataset for summer months (June–September) of 1998–2002 used for PFLOTRAN simulations: **(a)** daily evapotranspiration flux; **(b)** daily rain rate; and **(c)** cumulative daily rainfall.

HESSD
11, 12833–12882, 2014

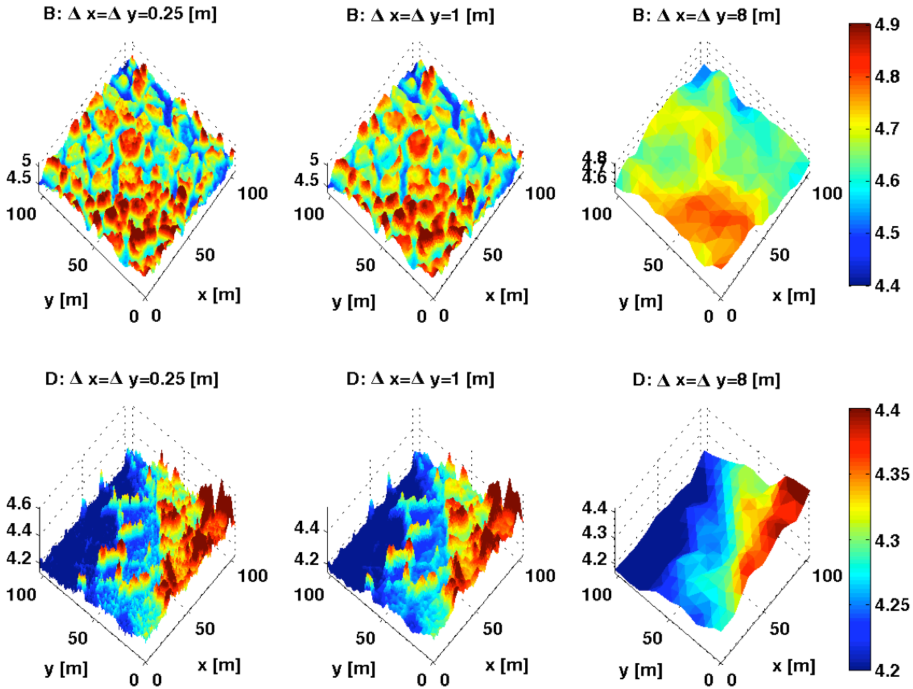

Figure 4. DEM for Site B (top row) and Site C (bottom row) at 0.25, 1, and 8 m resolutions.

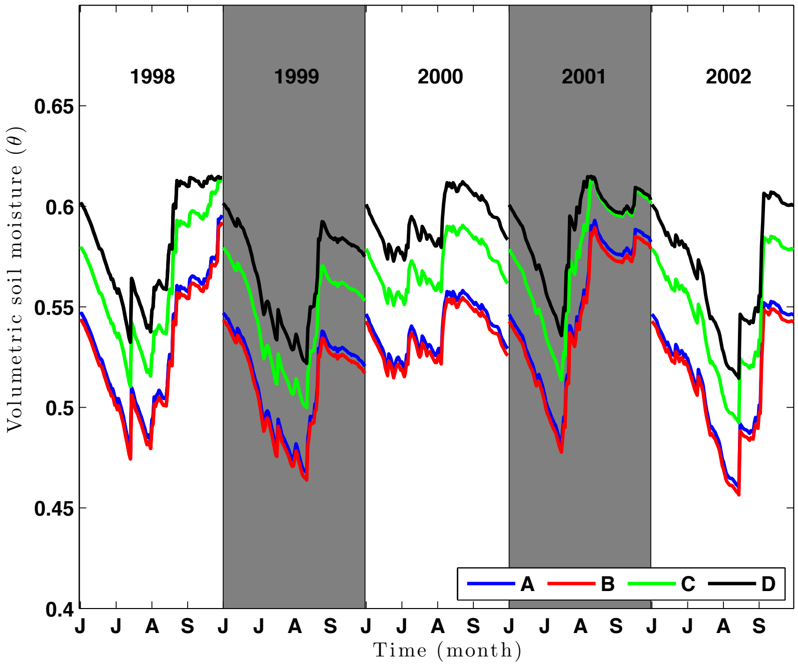

Figure 5. Time series of simulated mean soil moisture for the four NGEE-Arctic study sites.

HESSD
11, 12833–12882, 2014

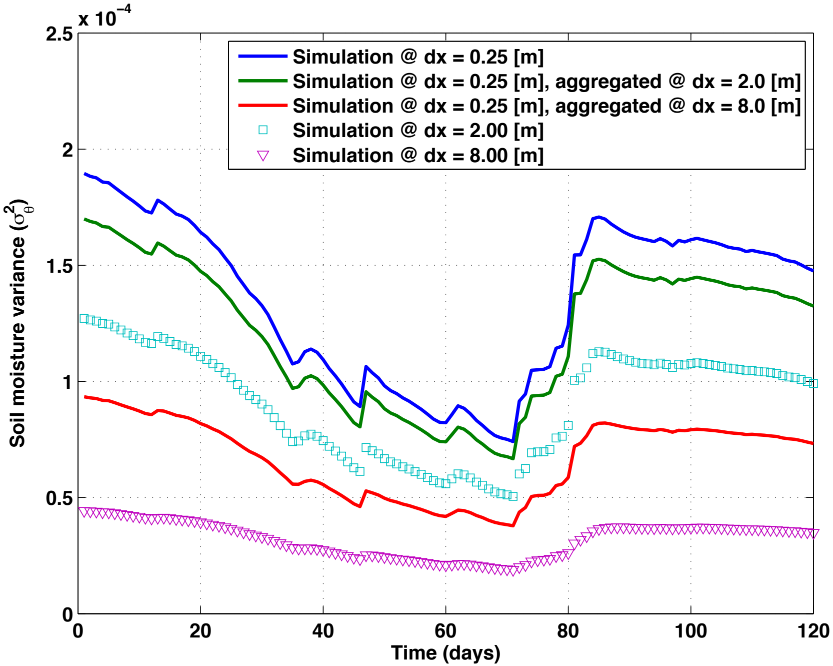

Figure 6. Time series of simulated soil moisture variance at site A for 1999 with PFLOTRAN mesh at the following resolutions: 0.25 m (blue line); 2.0 m (square symbols); and 8.0 m (triangle). Also, shown are time series for soil moisture variance obtained by coarsening the 0.25 m simulation results to 2 m (green line) and 8 m (red line).

HESSD
11, 12833–12882, 2014

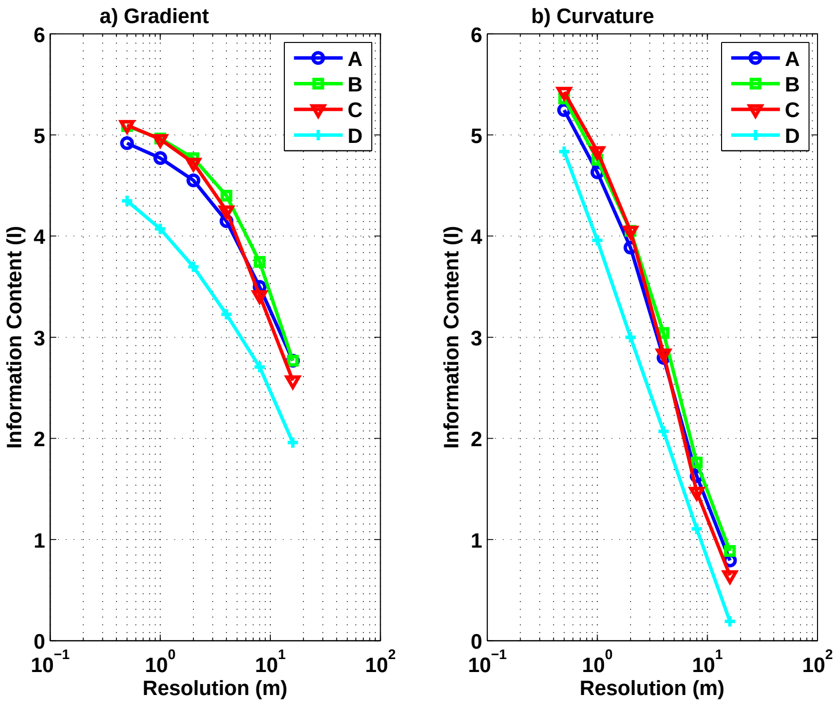

Figure 7. Information content vs. grid resolution for **(a)** gradient and **(b)** curvature for the four NGEE-Artic study sites.

HESSD
11, 12833–12882, 2014

Topographic controls on soil moisture scaling properties

G. Bisht and W. J. Riley

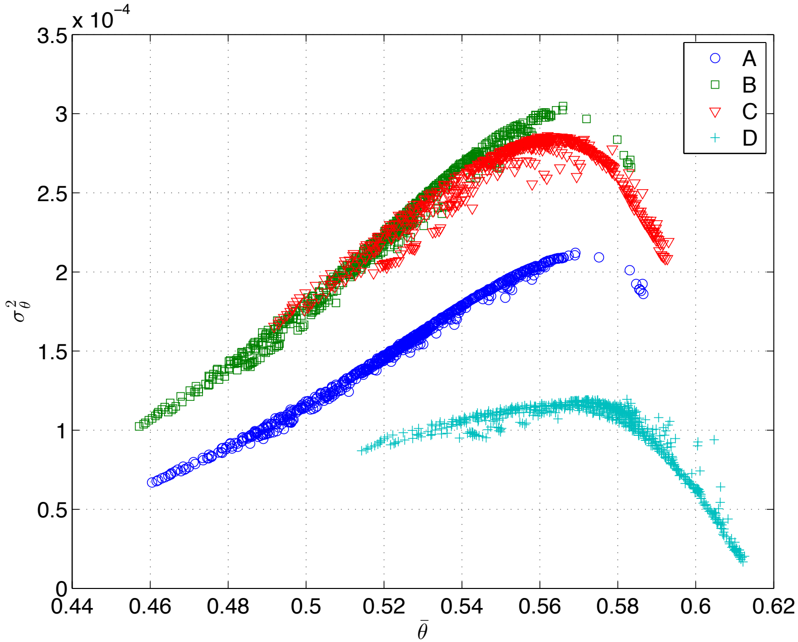

Figure 8. Soil moisture mean vs. variance at all four sites using finest resolution simulation for entire study period.

HESSD
11, 12833–12882, 2014

Topographic controls on soil moisture scaling properties

G. Bisht and W. J. Riley

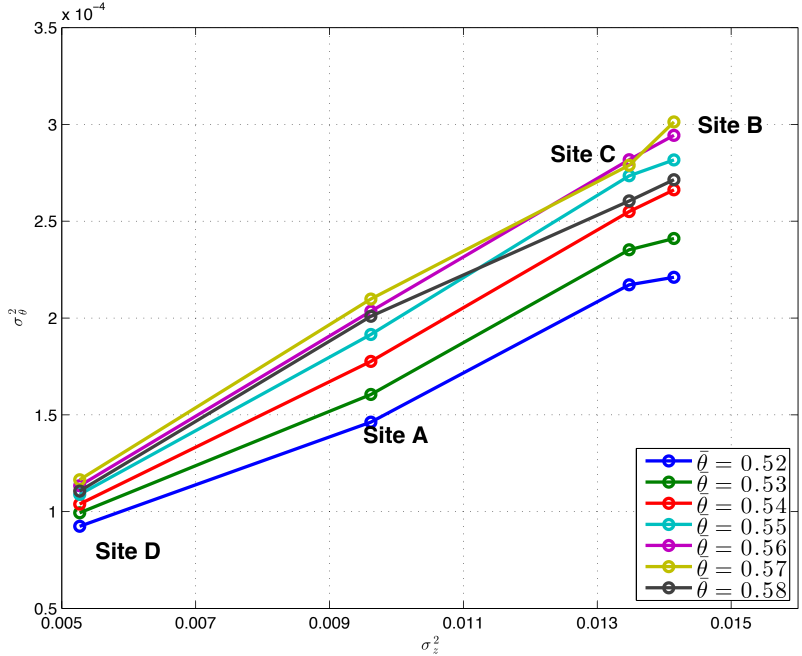

Figure 9. Simulated soil moisture variance vs. elevation variance at different mean soil moisture levels.

HESSD
11, 12833–12882, 2014

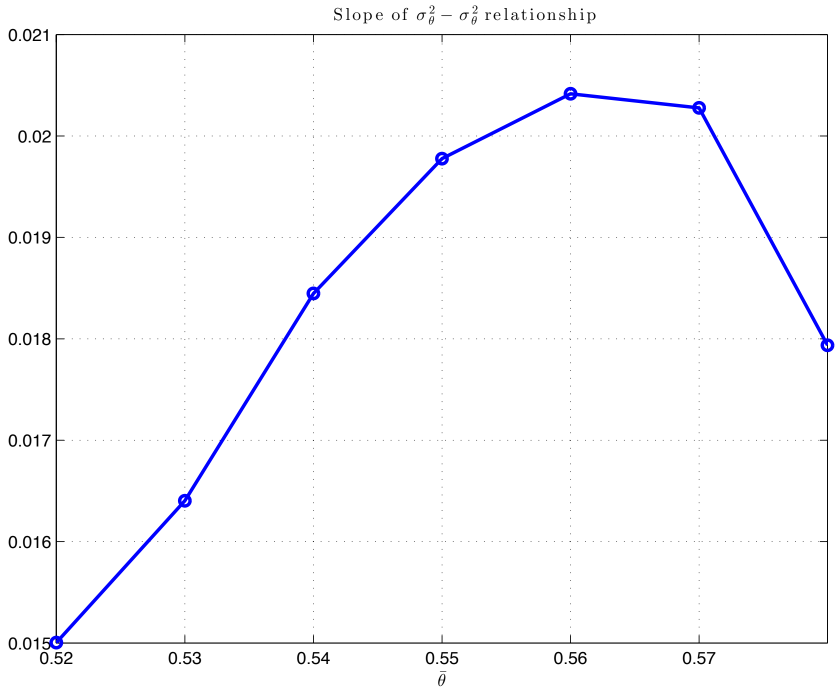

Figure 10. Slope of linear relationship between soil moisture variance – topography variance (computed from data presented in Fig. 9) vs. mean soil moisture bin.

HESSD
11, 12833–12882, 2014

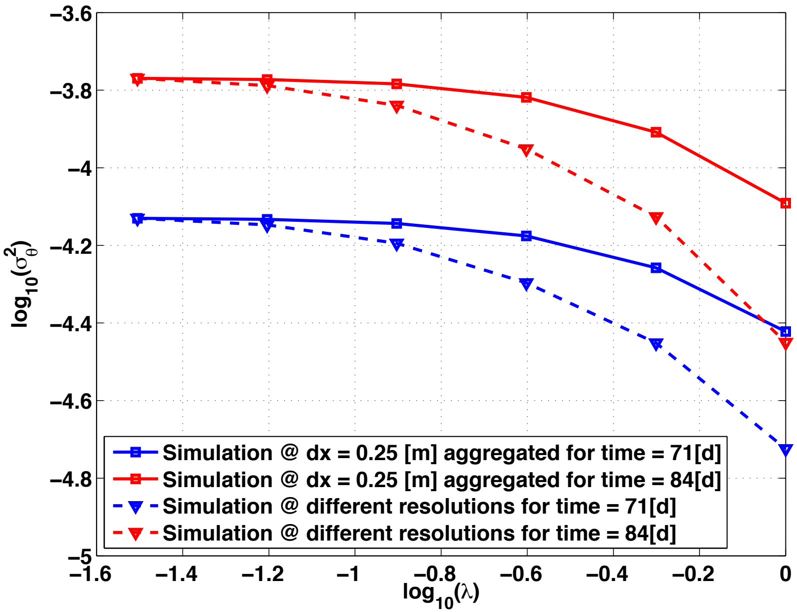

Figure 11. Soil moisture variance vs. scale factor for simulated soil moisture at Site-A for driest (blue) and wettest (red) day in 1999. A dashed line shows results obtained by performing PFLOTRAN at different spatial resolutions, while a solid line shows results obtained by aggregating 0.25 m PFLORAN simulation to coarser resolutions.

HESSD
11, 12833–12882, 2014

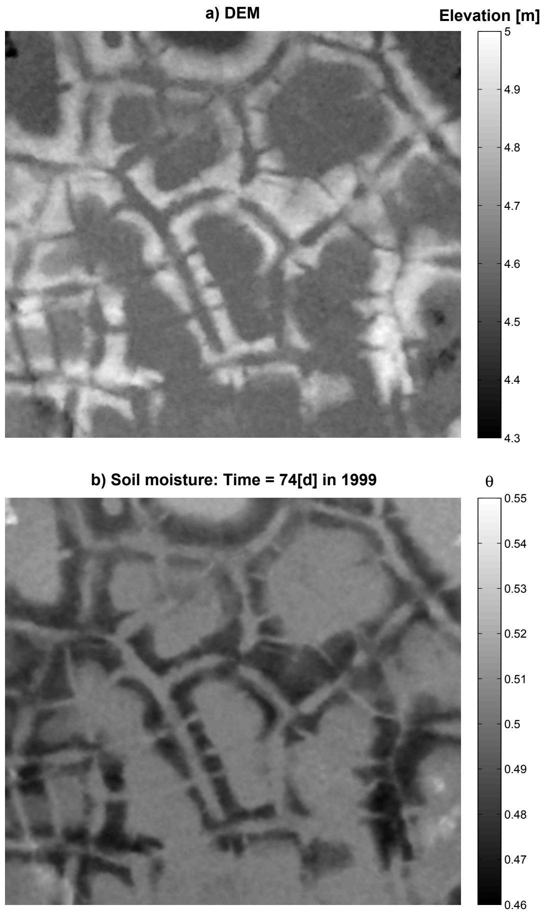

Figure 12. (a) DEM; and **(b)** simulated soil moisture distribution for driest day (t = 74 d) in 1999 at Site A.

HESSD
11, 12833–12882, 2014

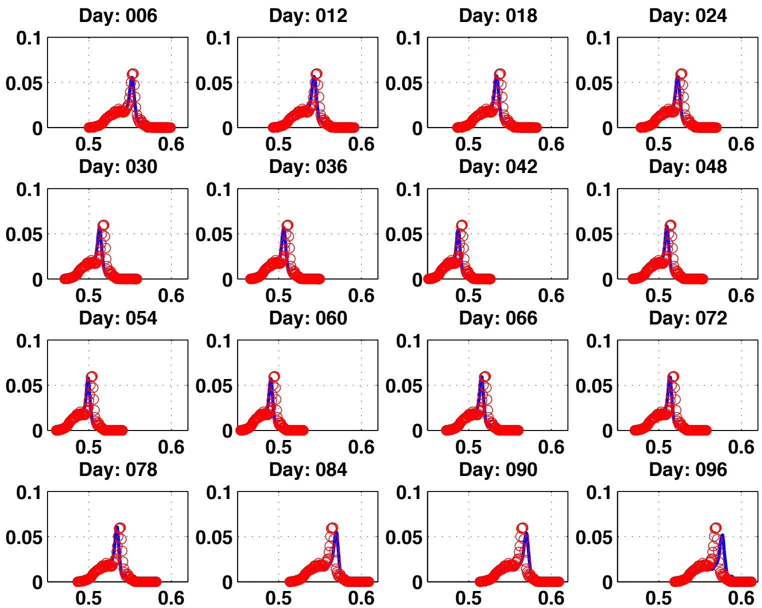

Figure 13. PDF for soil moisture at Site A for 1999 based on 0.25 m simulation (solid line) and inferred PDF using 8 m simulation (circle symbol).

HESSD
11, 12833–12882, 2014

Topographic controls on soil moisture scaling properties

G. Bisht and W. J. Riley

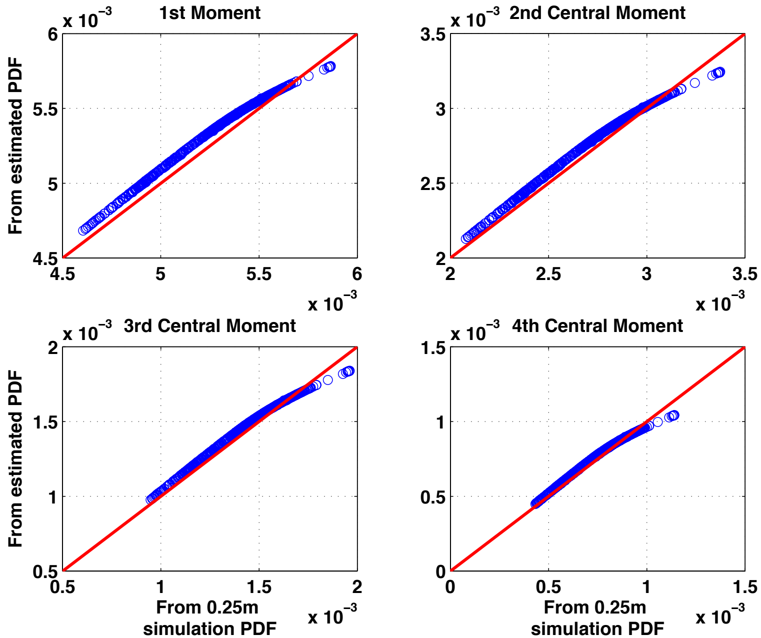

Figure 14. Comparison of soil moisture moments computed from estimated PDF and fine-scale simulations for Site A.

HESSD
11, 12833–12882, 2014

Topographic controls on soil moisture scaling properties

G. Bisht and W. J. Riley

Title Page
Abstract Introduction
Conclusions References
Tables Figures
Back Close
Full Screen / Esc
Printer-friendly Version
Interactive Discussion

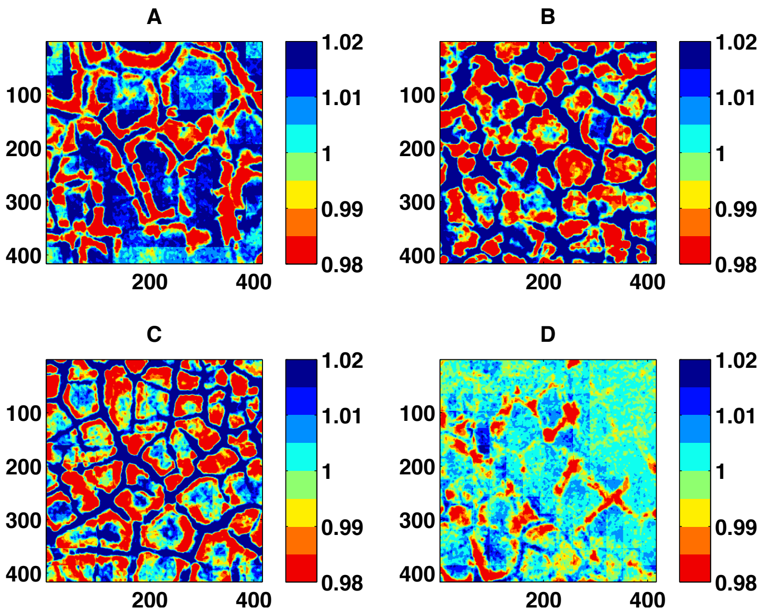

Figure 15. Mean downscaling factor for the four NGEE-Arctic sites.

HESSD
11, 12833–12882, 2014

Topographic controls on soil moisture scaling properties

G. Bisht and W. J. Riley

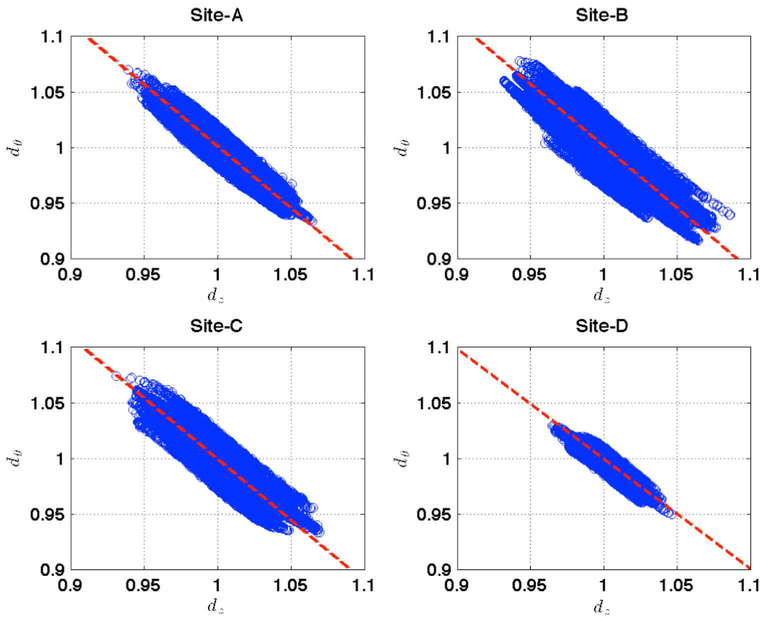

Figure 16. Linear relationship between downscaling factors for elevation (d_e) and soil moisture (d_θ) for all four NGEE-Arctic sites.

HESSD
11, 12833–12882, 2014

Topographic controls on soil moisture scaling properties

G. Bisht and W. J. Riley

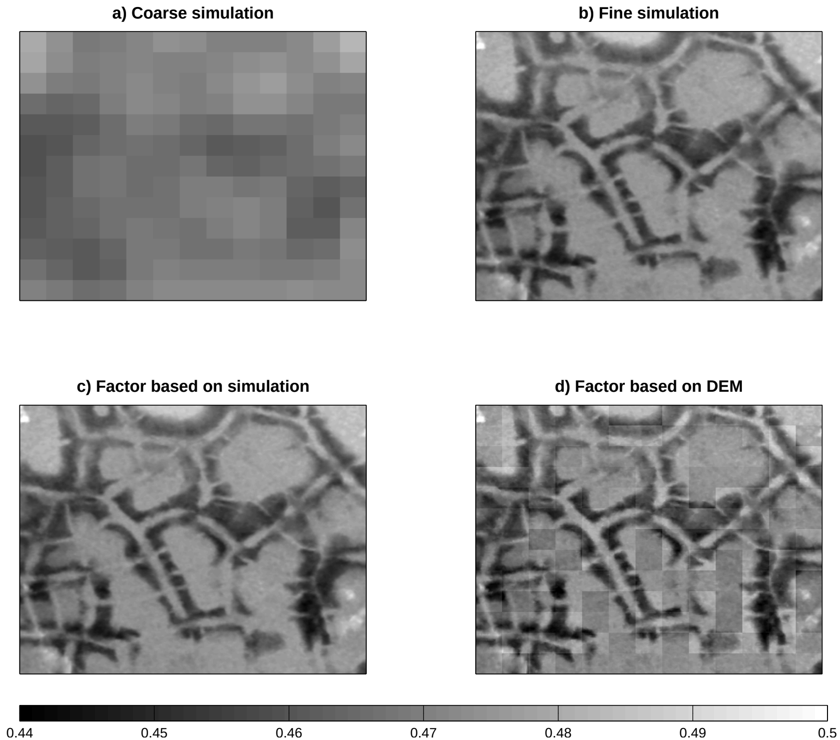

Figure 17. Simulated soil moisture for driest day (t = 74 d) in 1999 at Site A with **(a)** coarsest and **(b)** finest resolution DEM. Estimated fine-scale soil moisture pattern from 8 m simulation using downscaling factor obtained from **(c)** fine-resolution simulation and **(d)** fine-resolution DEM.

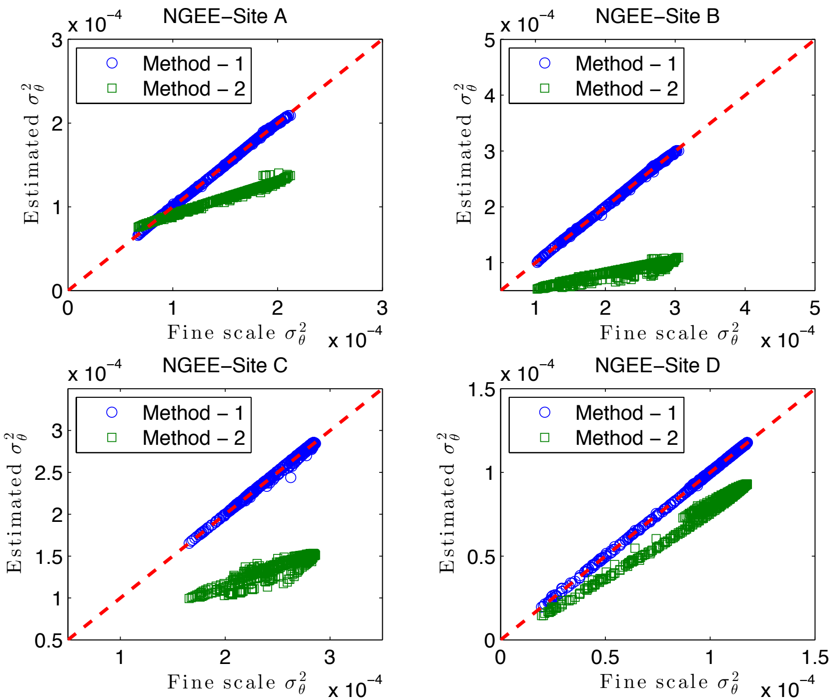

Figure 18. Comparison of simulated soil moisture variance obtained for DEM at 0.25 [m] with estimated soil moisture fields at finest resolution via two downscaling approaches.

HESSD
11, 12833–12882, 2014

Topographic controls on soil moisture scaling properties

G. Bisht and W. J. Riley

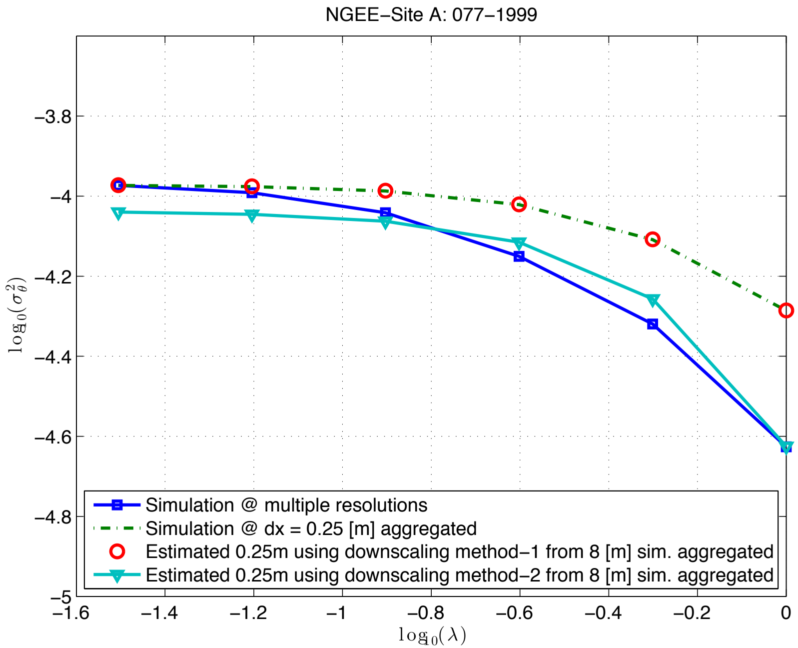

Figure 19. Soil moisture variance vs. scale factor for simulated soil moisture at Site A for the driest in 1999. Results are shown for (i) PFLOTRAN simulation at different spatial resolutions, (ii) aggregation of 0.25 m PFLORAN simulation to coarser resolutions, and aggregation of estimated fine-scale simulation obtained by (iii) first downscaling method and (iv) second downscaling method.

HESSD
11, 12833–12882, 2014

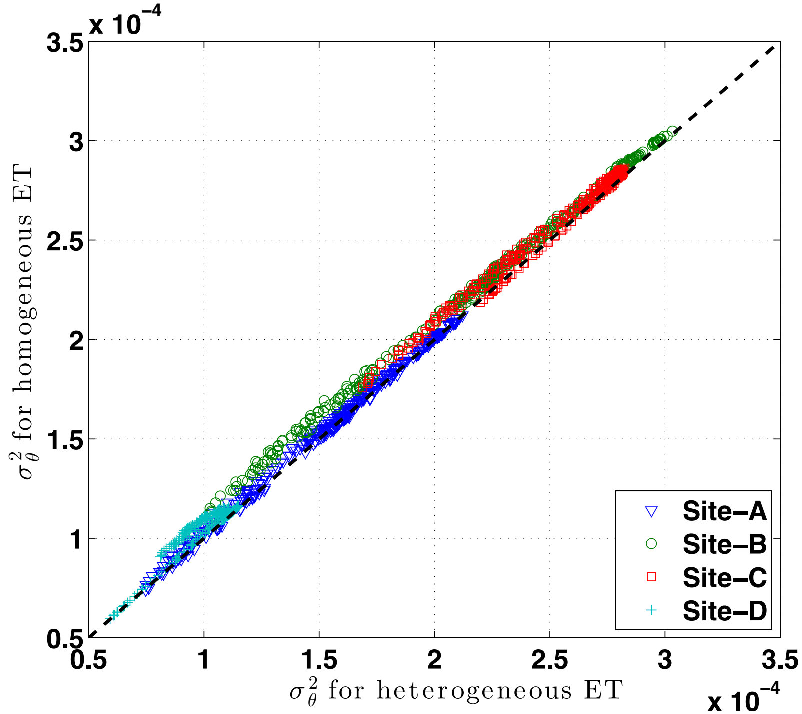

Figure 20. Comparison of simulated soil variance with and without vegetation heterogeneity for simulations performed at 0.25 [m].

HESSD
11, 12833–12882, 2014

Topographic controls on soil moisture scaling properties

G. Bisht and W. J. Riley